MODELLING OF COMPOSITE MANUFACTURING PROCESSES INCORPORATING LARGE FIBRE DEFORMATIONS AND PROCESS PARAMETER INTERACTIONS - EXAMPLE BRAIDING

B. Gröger*, J. Gerritzen, S. Eckardt, A. Gelencsér, E. Kunze, A. Hornig, R. Protz and M. Gude
Institute of Lightweight Engineering and Polymer Technology, Technische Universität Dresden, Dresden, Germany

*Corresponding author (benjamin.groeger@tu-dresden.de)

Keywords: Composite, Virtual Manufacturing, Finite elements

ABSTRACT

Braiding is a highly automated manufacturing technology for endless fibre reinforced composites, which are used for industrial applications with high requirements. The braiding process requires a complex tool concept and movement, which both significantly influence fibre paths and braiding angles and later on the final local fibre orientation and fibre volume fraction in the composite. This has in turn a pronounced impact on the resulting composite stiffness and strength. Besides the controllable process parameters, coefficients of friction and chosen fibre material can further affect the braiding angle. Within this paper, a modelling strategy for a braiding process is developed in order to investigate the effect of friction and mandrel geometry on the resulting braiding angle. Simulations both with a circular and a rectangular mandrel cross section and different friction coefficients between threads and tools are carried out. For a circular cross section, the results show no significant effect of friction, neither among threads themselves nor between threads and mandrel, on the braiding angle. On the mandrel with rectangular cross section, on the other hand, the coefficients of friction are strongly correlated with changes of the local braiding angle along plane areas and reduce rearrangements in the transitional areas.

1 INTRODUCTION

To fully exploit the potential of fibre reinforced composites (FRC), both an effective and highly automated manufacturing process is necessary and deviations from the originally specified reinforcement structure and uncertainties have to be quantified, especially when producing more complex components. The braiding process allows a continuous automated production of high quality parts. Furthermore, braiding can increase the industrial application due to the production of near net shaped preforms and subsequent combination with different manufacturing methods [1–4]. In particular, virtual process design enables a reduction of product development cycle time and ensures an effective manufacturing process. For this purpose, analytical [5] and kinematic [6] approaches have been developed to predict resulting braiding angle and fibre direction. These models can also take the interaction between the single threads into account [5]. Additionally, finite element (FE) modelling approaches for the braiding process have been developed. These investigations are mostly focused on complex braiding mandrels [7–9,9].

The most commonly used approach for discretising threads are beam chains or solid element formulations. The resultant fibre path can be used to generate structural models with geometrical cross-sections [10]. The modelling of a full length thread leads to dynamic effects caused by the motion of the bobbins. An efficient way to overcome this problem is a modelling setup proposed by [4]. Here, the bobbins are used as an element source generating a constant pretension analogous to the experimental setup. Most simulations assume a constant friction coefficient between thread and mandrel and the threads themselves. The results show a good qualitative agreement with the experimental results. In [7], a characterisation of the anisotropy of the friction coefficients between threads and core was carried out. The determined friction coefficients are implemented in the braiding simulation with a complex mandrel. A novel evaluation method allows for the analysis of the braiding angle around an entire cross

section of the mandrel. It can be seen, that the shape of the mandrel has a stronger influence on the braiding angle than the friction coefficient between the threads. The friction coefficient between the ring and the mandrel is assumed to be isotropic and constant. However, the influence of the friction between threads and mandrel as well as among the threads themselves in combination with the mandrel shape was not studied so far. Therefore, the presented investigation is focused on the analysis of the interaction between (I) tool and textile threads, (II) the threads with themselves depending on the shape of the mandrel.

2 PROCESS

The braiding setup contains a fixed number of bobbins with the used thread of the fibres. The bobbins are placed on a braiding wheel and move within the wheel along predefined paths around the mandrel in the centre (Fig. 1). Half of the bobbins move clockwise and the other half counterclockwise in circumferential direction in the braiding wheel. Due to the braiding setup of the wheel a vertical motion direction is used. Around the mandrel, a fixed braiding ring is installed to guide the fibres with a defined angle axial to the mandrel. The mandrel itself is moved in the axial direction to the braiding wheel. The circumferential velocity of the bobbins in the wheel and the axial velocity of the mandrel can be changed during the process to account for target braiding angle, degree of coverage or mandrel shape. The investigated setup of the horizontal braiding machine is illustrated in Fig. 1.

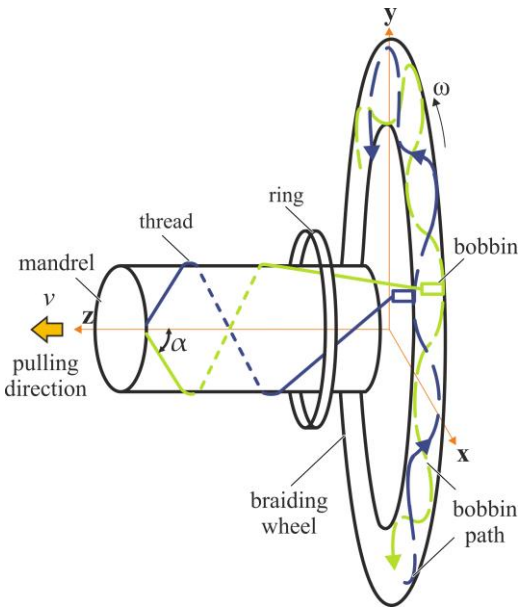

Fig. 1: Braiding setup with a vertical movement of the bobbins [11]

3 MODELLING

The virtual braiding process strategy is designed to predict the resulting braiding angle and fibre tensions, depending on the friction coefficient and mandrel shape using LS-Dyna. Therefore, the numerical description of the thread and the motion of the bobbins are focused.

3.1 Process characteristics

In the present work mandrels both with a cylindrical and a rectangular cross section and a length of 1000 mm are used. The dimensions of the cross sections are given in Fig. 2. The braiding process is carried out with 16 bobbins in a braiding wheel that is suitable for 48 bobbins. Furthermore, the ring in the braiding setup is neglected to reduce an additional friction source and model complexity. The spring loaded tensioning of threads at the bobbins is modelled as a constant pretension of 6.7 N.

a) cylindrical b) rectangular

Fig. 2: Cross section of the mandrels for braiding simulation.

The bobbins follow a circular path on the braiding wheel, with a radius R_b, superimposed with a sinusoidal oscillation with an amplitude R_c from the carrier wheels. The respective paths for clock- and counterclockwise movement are shown in Fig. 3.

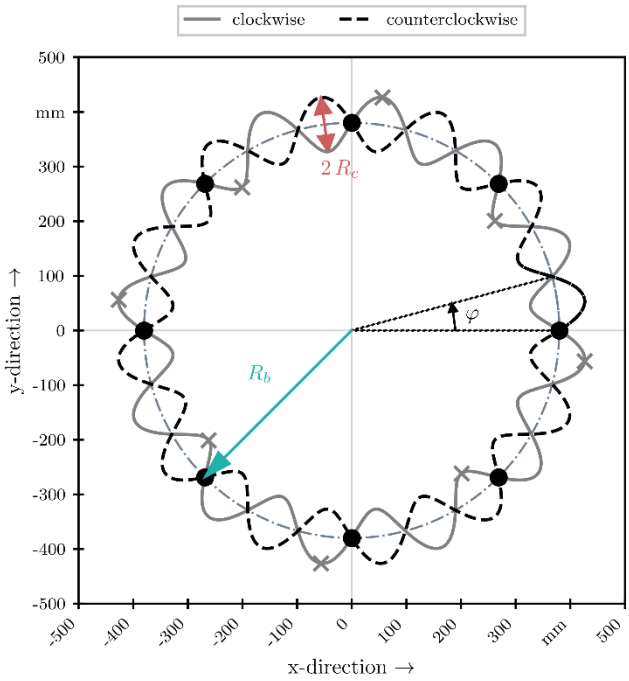

Fig. 3: Sinusoidal motion with amplitude R_c along radius R_b of the eight bobbins in counterclockwise direction (dashed black line) and clockwise (gray line). The initial position of the N bobbins (black circle for counterclockwise, gray cross for clockwise)

Therefore, the cartesian position of each bobbin is determined by its rotational direction and angle φ, which in turn depends on the angular velocity ω and past time t. The current radius position r of each bobbin can be given as

$$r_{ccw/cw}(\varphi) = R_b \pm R_c \, sin\left(N\frac{\varphi}{2}\right) \tag{1}$$

for counterclockwise and clockwise direction respectively, with the maximum numbers of bobbins N in the wheel. Given the ratio of used and possible bobbins, initially two bobbins are placed onto every third (16/48=1/3) carrier k ($k = 0, 3, \dots, 21$). All bobbins that move counterclockwise start on R_b, the bobbins moving clockwise start $R_b + (-1)^{k/3} R_c$. This is captured by an initial angular offset for the kth bobbin, depending on the direction of rotation: $\varphi_{ccw}^{k}|_{t=0} = \frac{2k\pi}{N}$ and $\varphi_{cw}^{k}|_{t=0} = \frac{(2k-1)\pi}{N}$. Due to the different directions of motion, separate equations relating angular velocity ω and rotation angles φ are required as per

$$\varphi_{ccw} = \omega \cdot t + \varphi_{ccw}^{k}|_{t=0} = \omega \cdot t + \frac{2\pi k}{N} \tag{2}$$

$$\varphi_{cw} = -\omega \cdot t + \varphi_{cw}^{k}|_{t=0} = -\omega \cdot t + \frac{(2k-1)\pi}{N}. \tag{3}$$

Based on the current radius position (Eqn. 1), and the rotational angle φ, the x- and y-position of every bobbin can be obtained using

$$x(\varphi) = r(\varphi)\, cos(\varphi) \quad (4)$$

$$y(\varphi) = r(\varphi)\, \sin(\varphi)\,. \quad (5)$$

By using Eqn. (1-5), the position of each bobbin at any arbitrary time t can be calculated. For subsequent simulation analyses, displacements and not positions are required. These are obtained by subtracting the initial x- and y-positions.

All relevant braiding process parameters are given in Table 1. Additionally an initial offset of the mandrel in axial direction of 145 mm is defined in accordance to the experimental setups.

Table 1: Relevant parameters for the braiding process simulation

Parameter	Value	Unit
Number of bobbins	16	
Number carriers N	24	
Braiding wheel radius R_b	380	mm
Carrier wheel radius R_c	50	mm
Angular velocity ω	0.6	s^{-1}
Target braiding angle α	±45	°
Pretension thread	6.7	N

3.2 Modelling setup

For the modelling of the threads a one-dimensional (1D) seat belt formulation with an initial thickness of 0.15 mm is used. The bobbins and the mandrel are discretised using rigid solid elements, additionally the mandrel surface is covered with shell elements to enable the usage of a forming contact definition between threads and mandrel surface allowing relative sliding. The contact among the threads themselves uses a penalty formulation. The numerical setup with the initial position of the bobbins at $t = 0$ s is presented in Fig. 4. The simulations are carried out with an explicit time integration scheme in LS-Dyna with 120 cores on five nodes of 2x Intel(R) Xeon(R) CPU E5-2680 v3 (12 cores) at 2.50 GHz with 64 GB RAM.

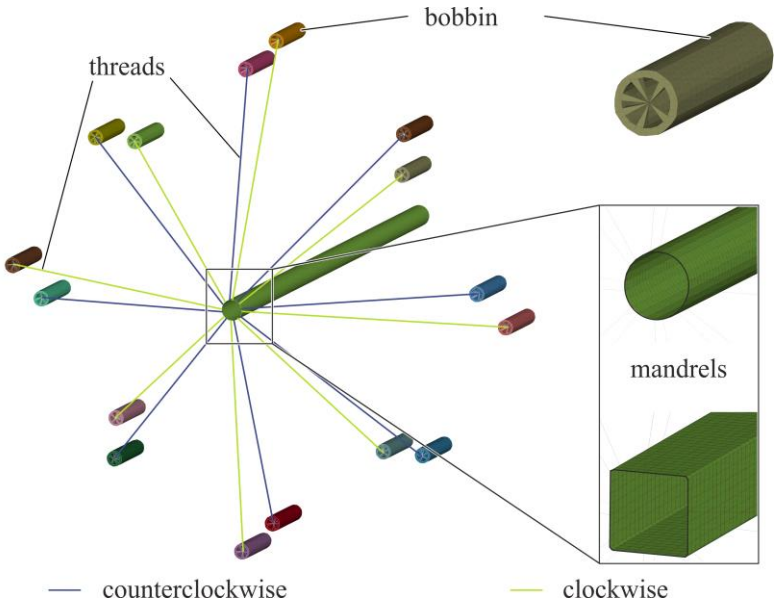

Fig. 4: Modelling setup a) in detail with mandrel, ring, bobbins, fixation plate and thread; b) overview of numerical model

The seat belt elements connecting two nodes with one degree of freedom (DOF) calculating tension

under mechanical load. The material behavior in axial direction is described directly by a force-strain curve with an equivalent stiffness of glass fibres. The pretensioning is modelled using seatbelt retractors at the bobbins, which remain in the "unlocked" state and thus allow pay-out of additional seat belt elements ("feeding elements") if the thread tension were to exceed the defined pretension. This approach allows for a significant reduction in computational cost by activating thread elements just in time, when they are actually needed.

The 1D seat belt elements for the circular mandrel have a characteristic element length l_e of 7 mm, whereas l_e for the rectangular mandrel is 2 mm for a more accurate contact description at the fillets in the corners. Therefore, potentials for 150 feeding elements for the circular and 1000 for the rectangular mandrel are defined. An overview of the two different numerical models is given in Table *2*. Boundary conditions, such as the angular velocity ω and the translational velocity v, were kept constant throughout all performed simulations.

In this work, the influence of two different coefficients of friction (COF) is investigated: Firstly, between mandrel and threads and secondly among the threads themselves. Both COFs are varied between 0.1 and 0.3.

Table 2: Characteristics of the numerical models for both mandrels

Number of	**Mandrel shape**	
	Circular	**Rectangular**
Nodes	39,642	63,404
Elements (total)	34,288	51,600
Elements (seat belt)	3,288	16,600
Elements (seat belt in each retractor)	150	1000

4 RESULTS

Variation of the coefficients of friction between mandrel and threads $\mu_{M\text{-}T}$ as well as among the threads themselves $\mu_{T\text{-}T}$ between 0.1 and 0.3 lead to a total of four simulations by combining $\mu_{T\text{-}T}/\mu_{M\text{-}T}$ with 0.1/0.1, 0.1/0.3, 0.3/0.1 and 0.3/0.3 per mandrel shape. For the circular mandrel, three full rotations of each bobbin around the mandrel and one rotation for the rectangular mandrel are evaluated. The braiding angle for every simulation is evaluated along each thread for all seat belt elements in contact with the mandrel. It is calculated by the dot product of the vector defined by the two nodes of each seat belt element and the mandrel axis. As opposed to evaluating discrete points, this allows for a continuous evaluation of the braiding angle along the entire covered mandrel, which is especially important for complex mandrel shapes. The evaluation is automated using the Python library 'LASSO-Python' for extracting node coordinates from 3dplot results files. The calculation of thread orientation vectors and braiding angles is carried out with 'NumPy' [12] and 'pandas' [13] .

4.1 Evaluation of the braiding angle for the circular mandrel

The resulting braiding pattern for $\mu_{M\text{-}T} = \mu_{T\text{-}T} = 0.1$ is shown in Fig. 5. The patterns for the other configuration are similar. A homogenous braiding pattern around the mandrel can be seen. Given the characteristic element length l_e of 7 mm, the circular shape of the mandrel is reproduced accurately.

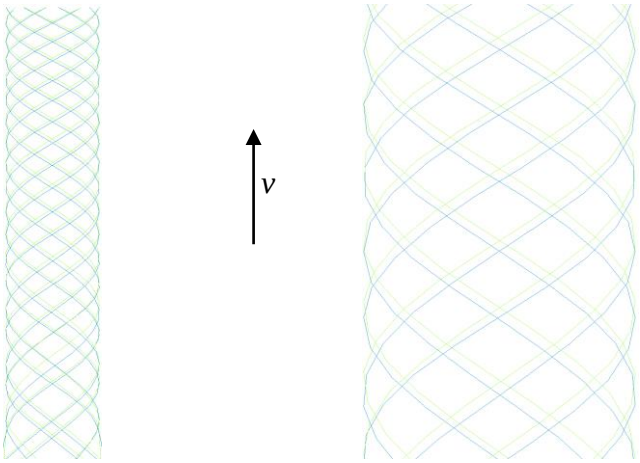

a) Threads after 3 rotations b) Detailed view

Fig. 5: Results of the braiding simulation after 3 rotations of the bobbins a) braiding pattern and b) detailed view of the braiding pattern

The orientation of each thread in the four simulations and the resulting curve are presented in Fig. 6a. The braiding angle decreases with progressing process for all configurations similarly. The change of the braiding angle can be attributed to the increasing braiding distance Δz between the bobbins and the last contact point of thread and mandrel (Fig. 6b).

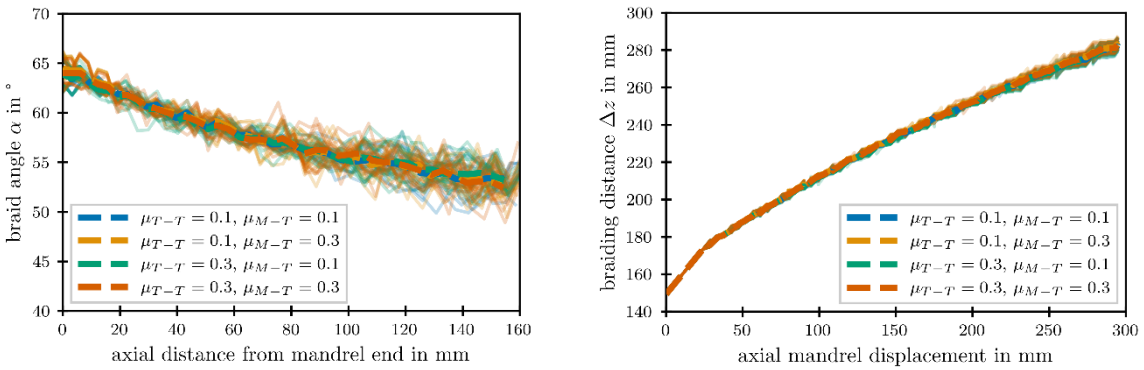

a) b)

Fig. 6: Results for the four different configurations using the circular mandrel: a) braiding angle α and b) braiding distance Δz

From this, it can be concluded that neither coefficient of friction has a significant effect on the resulting orientation.

4.2 Evaluation of the braiding angle for the rectangular mandrel

The simulation of the four friction coefficient configurations with the rectangular mandrel are carried out with the same initial and boundary conditions as the ones with circular mandrel. The resulting braiding pattern for for $\mu_{M\text{-}T} = \mu_{T\text{-}T} = 0.1$ after one rotation of the bobbins is presented in Fig. 7. At the beginning of the simulation, dynamic oscillations of the threads can be observed. These decay rapidly with progression of the braiding process and the associated increase in the interactions among the threads.

A detailed analysis of the braiding angles for each thread element within the four different configurations is shown in Fig. 8. From the figure it becomes clear that the initial orientations vary and the braiding angle decreases with progression of the braiding process, similar to the results with circular mandrel. Areas of constant braiding angle can be identified, corresponding to the four faces of the profile. The significant changes of the braiding angle therefore result from the edges.

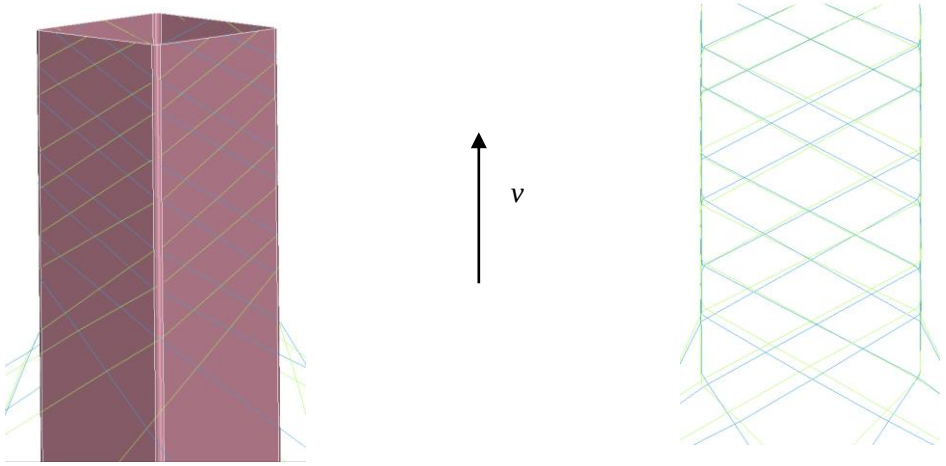

Fig. 7: Results of the braiding simulation after one rotation of the bobbins a) detailed view of the braiding pattern with mandrel and b) braiding pattern

Due to the flat faces and the edges with a radius of 1.2 mm, the threads can slide along the face until the thread is bent over the next edge. This can be attributed to the fact that no significant normal force of the thread acts against the mandrel plane. Hence, the friction between the mandrel – threads as well the interaction between the threads themselves play a major role regarding the resulting local braiding angle. Due to the pretension of the threads, caused by the bobbins, normal forces occur when threads are in contact. Especially at the edges these interactions significantly influence the tendency of threads to slide or stick. Hence, a small coefficient of friction between mandrel and thread leads to sliding and a higher difference of braiding angles between adjacent faces (Fig. *8*a-b). In Fig. *8*b ($\mu_{M\text{-}T} < \mu_{T\text{-}T}$) more sliding occurs, especially at the edges, which can lead to a reorientation of adjacent thread sections. In Fig. *8*c-d the edge sliding is reduced due to the high value of $\mu_{M\text{-}T}$.

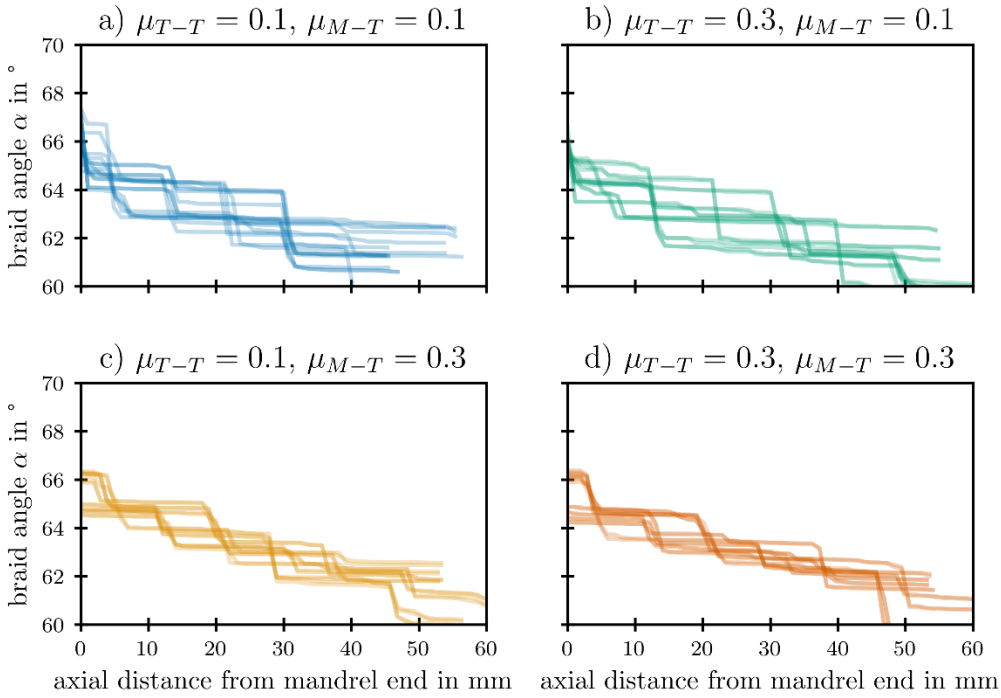

Fig. 8: Braiding angles along each thread while in contact with the mandrel

5 CONCLUSION

A modelling strategy to simulate the braiding process with glass fibre yarns has been proposed. It is intended to use results of such simulations to adjust and control the braiding process parameters in a virtual manner before physical trials, thus minimizing costly process and manufacturing setup iterations. Especially for non axisymmetrical mandrels this modelling strategy enables a detailed process understanding. It has been shown, that the elaborated simulation strategy is principally suited to conduct braiding process evaluations virtually using the commercial FE Software LS-Dyna. Furthermore, it has been shown that a discrete evaluation method of the braiding angle can lead to misleading results and conclusions for the process. Additionally, the influence of two coefficients of friction, mandrel-thread and thread-thread, and the mandrel shape on the resulting braiding angle and pattern was investigated. For a circular mandrel no significant change of the braiding angle can be observed. For a rectangular mandrel, however, the friction coefficient has a significant influence on the resulting fibre path. Hence, the approach is sensitive to friction coefficients and can also be used to investigate different process and tool parameters. With the proposed modelling strategy neither the degree of coverage can be identified nor the crimp of the threads. Due to the contact definition between the threads and tool the discretization level of the threads plays a major role for braiding simulations. Therefore, in further work shell seat belt elements will be used for a spatial definition of the thread width and additional consideration of bending and compression behaviour.

ACKNOWLEDGEMENTS

The authors are grateful to the Center for Information Services and High Performance Computing [Zentrum für Informationsdienste und Hochleistungsrechnen (ZIH)] at TU Dresden for providing its facilities for high throughput calculations.

FUNDING

This research was funded by the German Research Foundation (DFG) within the projects Transregional Collaborative Research Centre 285 (TRR 285) (project number 418701707) sub-project A03 for the rotational-symmetrical case and 428328210 for the non-rotational symmetrical case.

REFERENCES

[1] Advances in Braiding Technology, Elsevier, 2016.
[2] D. Barfuss, R. Grützner, F. Hirsch, M. Gude, R. Müller, M. Kästner, Multi-scale structuring for thermoplastic-metal contour joints of hollow profiles, Prod. Eng. Res. Devel. 12 (2018) 229–238. https://doi.org/10.1007/s11740-018-0800-9.
[3] J. Schäfer, T. Gries, Braiding pultrusion of thermoplastic composites, in: Advances in Braiding Technology, Elsevier, 2016, pp. 405–428.
[4] X. Sun, L.F. Kawashita, T. Wollmann, S. Spitzer, A. Langkamp, M. Gude, Experimental and numerical studies on the braiding of carbon fibres over structured end-fittings for the design and manufacture of high performance hybrid shafts, Prod. Eng. Res. Devel. 12 (2018) 215–228. https://doi.org/10.1007/s11740-018-0824-1.
[5] M. Imbert, H. Finckh, G.T. Gresser, Mechanical analytical modelling of non-axisymmetric overbraiding, Journal of Composite Materials 55 (2021) 1385–1404. https://doi.org/10.1177/0021998320968625.
[6] J.F.A. Kessels, R. Akkerman, Prediction of the yarn trajectories on complex braided preforms, Composites Part A: Applied Science and Manufacturing 33 (2002) 1073–1081. https://doi.org/10.1016/S1359-835X(02)00075-1.
[7] T. Hans, J. Cichosz, M. Brand, R. Hinterhölzl, Finite element simulation of the braiding process for arbitrary mandrel shapes, Composites Part A: Applied Science and Manufacturing 77 (2015) 124–132. https://doi.org/10.1016/j.compositesa.2015.06.003.
[8] S. Kim, Simulation of maypole braiding process with multi-layer interlocking yarns, The Journal of The Textile Institute 108 (2017) 579–585. https://doi.org/10.1080/00405000.2016.1176621.

[9] W.-J. Na, H.C. Ahn, S.-Y. Jeon, J.S. Lee, H.-M. Kang, W.-R. Yu, Prediction of the braid pattern on arbitrary-shaped mandrels using the minimum path condition, Composites Science and Technology 91 (2014) 30–37. https://doi.org/10.1016/j.compscitech.2013.11.012.
[10] A.K. Pickett, J. Sirtautas, A. Erber, Braiding Simulation and Prediction of Mechanical Properties, Appl Compos Mater 16 (2009) 345–364. https://doi.org/10.1007/s10443-009-9102-x.
[11] X. Hu, Y. Zhang, Z. Meng, Y. Sun, Tension modeling and analysis of braiding carriers during radial-direction and axial-direction braiding, The Journal of The Textile Institute 110 (2019) 1190–1201. https://doi.org/10.1080/00405000.2018.1550871.
[12] C.R. Harris, K.J. Millman, S.J. van der Walt, R. Gommers, P. Virtanen, D. Cournapeau, E. Wieser, J. Taylor, S. Berg, N.J. Smith, R. Kern, M. Picus, S. Hoyer, M.H. van Kerkwijk, M. Brett, A. Haldane, J.F. Del Río, M. Wiebe, P. Peterson, P. Gérard-Marchant, K. Sheppard, T. Reddy, W. Weckesser, H. Abbasi, C. Gohlke, T.E. Oliphant, Array programming with NumPy, Nature 585 (2020) 357–362. https://doi.org/10.1038/s41586-020-2649-2.
[13] The pandas development team, pandas-dev/pandas: Pandas, Zenodo, 2023.